Miner Deposita (2006) 41: 281–295
DOI 10.1007/s00126-006-0059-5

ARTICLE

Damian S. Smith · Ian J. Basson

Shape and distribution analysis of Merensky Reef potholing, Northam Platinum Mine, western Bushveld Complex: implications for pothole formation and growth

Received: 9 May 2005 / Accepted: 26 March 2006 / Published online: 27 April 2006

Abstract Syn-magmatic removal of the cumulate pile during the formation of the Bushveld Complex resulted in "potholes". Erosion progressed downward in the cumulate pile, resulting in a series of steep, transgressive contacts between locally conformable potholed reefs in the regional pothole sub-facies of the Swartklip Facies in the western limb of the Bushveld Complex. The deepest of these potholes, "third-order" or "FWP2" potholing, occurs where the base of the Merensky Cyclic Unit transgresses the Upper Pseudo-Reef Chromitite marker horizon. The base of a FWP2 pothole on Northam Platinum Mine consists of an unconformable stringer Merensky Chromitite overlain by a medium-grained, poikilitic orthopyroxenite and underlain by either a pegmatitic harzburgite or the medium-grained Lower Pseudo-Reef Anorthosite. Detailed shape and distribution analysis of FWP2 potholes reveals underlying patterns in their shape and distribution which, in turn, suggest a structural control. The ratio between pothole short vs long axes is 0.624 (N=1,385), although the ratio increases from 0.48 to 0.61 in the long axis range 10 to 60 m, then decreases from 0.61 to 0.57 from 61 to 100 m, increasing again from 0.57 to 0.61 from 101 to 400 m, suggesting that there is not a simple relationship between pothole shape and size. Shape (circularity, eccentricity, and dendricity) analysis of a subset of 638 potholes indicates that potholes with long axes <100 m have an elliptical, average normalized shape, elongate on a 120–150° orientation. Potholes with long axis lengths >100 m have an average normalized shape that is bilobate and elongate on a 120° orientation. The average aspect ratio (short axis length divided by long axis length) of potholes is highest for potholes with long axis lengths >100 m and lowest for potholes with long axis lengths between 35 and 60 m. The most common long axis orientation for potholes with long axis lengths <100 m is 150° but 120° for long axis lengths >100 m. Fractal analysis indicates that the distribution of pothole centers is controlled neither by a single nor several interacting fractal dimensions. Autocorrelation (Fry) analysis of the distribution of pothole centers shows recurring pothole distribution trends at 038, 070, and 110° for potholes over the full range of long axis lengths, while the trends of 008 and 152° occur in potholes with long axes lengths between 60 and 100 m. Chi-squared (X^2) analysis of the locations of pothole centers suggests that the distribution of small potholes is highly non-uniform but becomes exponentially more uniform with increasing pothole size. The model which best fits the observed shape and distribution analysis is a combination of protracted independent growth and "nearest neighbor" merging along specific orientations. For instance, the clustered distribution of original pothole centers resulted in merged potholes with long axes lengths of up to 60 m, exhibiting short vs long axes ratios of 0.61, preferred orientations of 150°, and alignment along 010 and 150° trends. Further independent growth allowed for merging of similar-sized (and smaller) neighboring potholes, generating potholes with long axes of up to 100 m in length, a preferred long axis orientation of 150°, and alignment along 010, 040, 075, and 150°. Subsequent preferential merging occurred along a 120° trend, thereby preserving a bilobate form. This implies that while pothole initiation and enlargement may be driven by a "top-down" (i.e., possibly thermomechanical) process, an underlying linear or structural catalyst/control is revealed in changes in pothole shape during enlargement and, furthermore, in the preferred trends along which potholes merged over a

Editorial handling: B. Lehmann

D. S. Smith
Northam Platinum Mine,
P.O. Box 441 Thabazimbi, 1380, South Africa
e-mail: dsmith@norplats.co.za

I. J. Basson (✉)
Department of Geological Sciences, University of Cape Town,
Private Bag Rondebosch,
Cape Town, 7701, South Africa
e-mail: ianbasson@tect.co.za

Present address:
I. J. Basson
Tect Geological Consulting,
1st Floor, 15 Rue le Havre,
Monte Sereno, Somerset West, 7130, South Africa

considerable period, possibly concomitant with adjustment of major structures in the footwall to the Bushveld Complex and pulses into the magma chamber.

Keywords Bushveld Complex · Merensky Reef · Potholes

Introduction

Regional geology

The Rustenburg Layered Suite of the Bushveld Complex contains several mineralized horizons, the Merensky Reef being the best documented of these due to its economic importance (Von Gruenewaldt 1977; Eales et al. 1993; Lee 1996; Viljoen 1994, 1999). Viljoen (1999) broadly defined the reef as "a mineralized zone within or closely associated with an unconformity surface in the ultramafic cumulate at the base of the Merensky Cyclic Unit (MCU)". Cawthorn and Boerst (2002) suggested that the MCU comprises a lower chromitite horizon, a feldspathic pyroxenite that may exhibit a lower pegmatitic portion with a thin chromitite stringer, followed by a thin layer of norite, in turn followed by a layer of anorthosite. The basal chromitite of the MCU has also been termed a "post-erosional cumulate drape" as its platinum group element (PGE) content, thickness, and overall texture are largely constant, regardless of the thickness of the reef and its variably recrystallized footwall lithologies (Smith et al. 2004).

Ongoing research has highlighted the remarkable variability in the Merensky Reef's petrographic character, thickness, and stepped, transgressive nature with respect to the layered cumulates of the Upper Critical Zone (UCZ) (Kruger and Marsh 1982; Ballhaus 1988; Kruger 1990, 1994; Carr et al. 1994a,b; Viljoen 1999; Wilson and Chunnett 2002; Smith et al. 2004). Modeling and prediction of this transgressive aspect are crucial during mining, which targets planar, conformable Merensky Reef. The reef has consequently been subdivided into several facies, sub-facies and types to provide local classification schemes for mining in the western limb of the Bushveld Complex (Fig. 1). Two facies have been identified, based on the stratigraphic thickness of UCZ units, the proportion of olivine-bearing rock types and mineralogical and geochemical trends (Wagner 1929; Eales and Cawthorn 1996; Maier and Eales 1997; Viljoen 1999), namely, the Rustenburg and Swartklip Facies. Viljoen (1994) further subdivided the Rustenburg Facies into four sub-facies or reef types (Contact Reef, Rolling Reef, Potholed Thin Reef and non-pegmatitic wide reef) and the Swartklip Facies into two sub-facies or reef types (Normal Reef and Regional Pothole Reef).

The Normal Reef sub-facies (Viljoen 1994) occurs where the base of the MCU does not transgress the lower chromitite of the Merensky Normal Reef (Viring and Cowell 1999; Cawthorn and Boerst 2002; Smith et al. 2004; Fig. 2), whereas regional-scale (>10^3 m^2) transgressions of this lower chromitite by the base of the MCU comprise the Regional Pothole sub-facies (Fig. 2; Viljoen 1999; Smith et al. 2004). Smaller-scale (<10^3 m^2) stepped variations in the elevation of the base of the MCU with respect to the underlying stratigraphy have led to the definition of several localized reef types and transition zones (Viljoen 1994, 1999; Viring and Cowell 1999; Fig. 2).

Whereas the transgressive nature of potholes, their vertical morphology with respect to the cumulate stratigraphy, and the positive correlation between aerial extent and depth have been well documented (e.g., Lee 1981; Viljoen 1994; Viljoen et al. 1986a,b; De Bruin 2002), their morphology in plan view has been primarily qualitatively described as being circular, ovoid, elongate, amoeboid, or irregular, with potholes displaying largely random orientations and distributions (Viljoen et al. 1986a,b; Viljoen and Hieber 1986; Leeb-Du Toit 1986; Farquhar 1986; Mossom 1986). Carr et al. (1994a,b), however, proposed that the orientations and siting of potholes are related to minor listric faulting in the floor/basement to the Bushveld Complex.

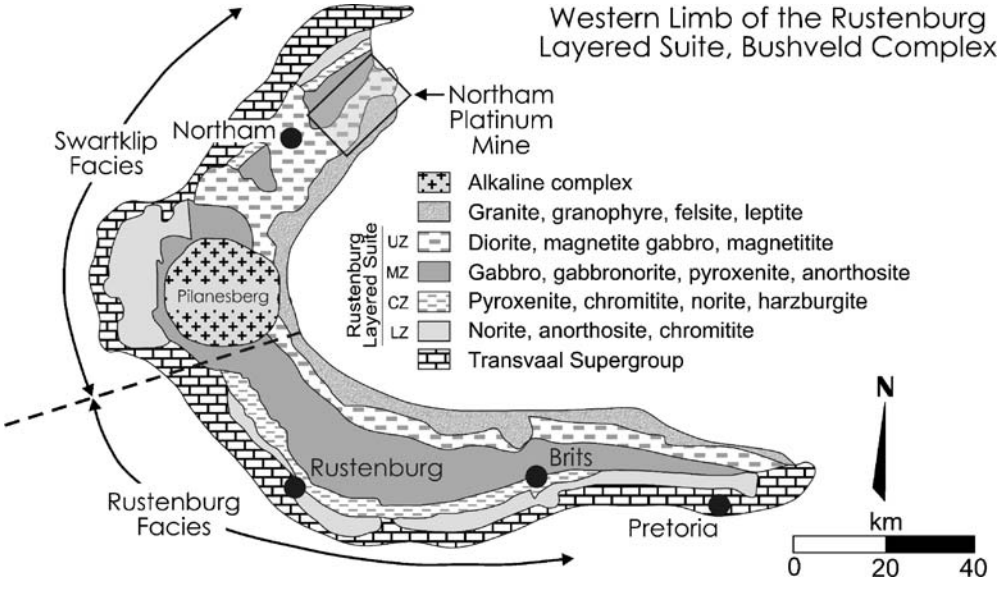

Fig. 1 The western limb of the Bushveld Complex, showing its two main facies (Wagner 1929), and the form of the Rustenburg Layered Suite (RLS). The study area, the Northam Platinum Mine, is located north of the Pilanesberg Complex in the Swartklip Facies (modified after Viljoen 1994, 1999)

Regional Pothole sub-facies at Northam

Northam Platinum Mine exploits the Normal Reef sub-facies (Smith et al. 2004) and those portions of the Regional Pothole sub-facies where the base of the MCU is conformable to the underlying stratigraphy (Viring and Cowell 1999). The Regional Pothole sub-facies at Northam has been divided into three reef types, two of which comprise conformable to paraconformable mineralized horizons, separated from each other and the Normal Reef sub-facies by unconformable transition zones (Fig. 2). The upper conformable mineralized horizon, analogous to "first-order potholing" (Viring and Cowell 1999), occurs at the Footwall Marker (Viljoen et al. 1986a; Eales and Reynolds 1986) and is termed the NP2 Reef at Northam (Viring and Cowell 1999; Fig. 2). This reef comprises a mineralized stringer (Merensky) chromitite, overlain by a medium-grained, poikilitic orthopyroxenite and underlain by a variably "troctolized" leucocratic footwall (Fig. 3a; Viljoen et al. 1986a; Viring and Cowell 1999). Mineralization extends for up to 30 cm above and up to 120 cm below the stringer chromitite, depending upon the nature of the immediate footwall.

The lower conformable mineralized horizon, analogous to "second-order potholing" (Viring and Cowell 1999), includes the Upper Pseudo-Reef (P2) chromitite (Viljoen et al. 1986a; Eales and Reynolds 1986). This is termed the P2 Reef at Northam (Viring and Cowell 1999), comprising two stringer chromitites (Merensky and Upper Pseudo-Reef) which are typically separated by approximately 50 cm of pegmatitic pyroxenite. The upper (Merensky) chromitite is overlain by a medium-grained poikilitic orthopyroxenite, while the lower chromitite is underlain by the pegmatitic "Tarentaal" harzburgite. Mineralization extends up to 30 cm into the hanging wall of the Merensky Chromitite and up to 80 cm into the footwall of the Upper Pseudo-Reef Chromitite (Fig. 3b).

The lowermost reef type, analogous to "third-order potholing" (Viring and Cowell 1999), is defined where the base of the MCU transgresses the Upper Pseudo-Reef (P2) chromitite (Fig. 3c). This is referred to, in this study, as FWP2 potholing (Viring and Cowell 1999). In these areas, an unconformable stringer (Merensky) chromitite is overlain by a medium-grained poikilitic orthopyroxenite and underlain by either a pegmatitic "Tarentaal" harzburgite or the medium-grained Lower Pseudo-Reef anorthosite (Eales and Reynolds 1986). Mineralization is highly variable and can extend up to 80 cm above and up to 150 cm below the Merensky Chromitite. The inherent irregularity in mineralization makes mining of FWP2 problematic.

The aim of this study is to characterize the shape and the distribution of local, third-order (i.e., FWP2) potholes. This is to determine whether there are any underlying patterns or trends. This characterization allows us to propose a model for the initiation and growth of third-order potholing using the postulate of thermomechanical erosion as the mechanism of

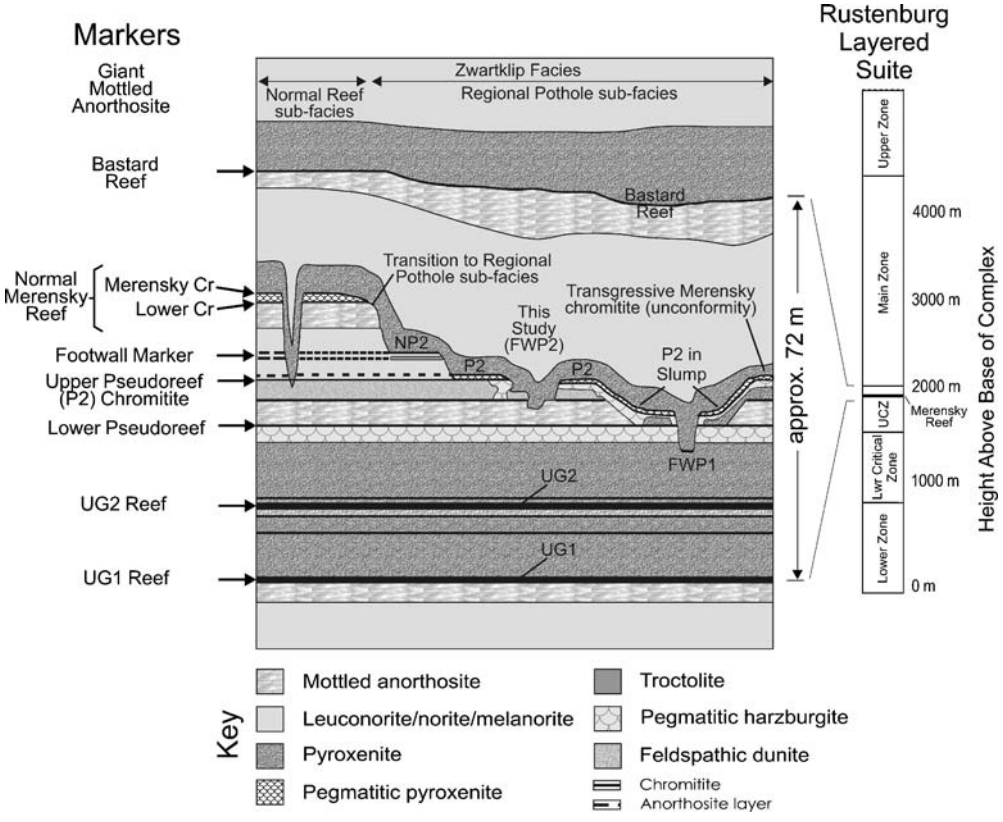

Fig. 2 Schematic cross-section of the upper portion of the Upper Critical Zone of the RLS, at Northam Platinum Mine. The Normal Reef sub-facies occurs where the Merensky Reef is in its normal stratigraphic position, whereas the Regional Pothole sub-facies starts where the base of the MCU transgresses the lower chromitite (locally termed "4X") of the Merensky Normal Reef. Reef types in the Regional Pothole sub-facies are defined where the Merensky Cyclic Unit is conformable to footwall lithologies. Transitions between reef types occur where the Merensky Cyclic Unit truncates the underlying stratigraphy. This study focuses on the deepest commonly occurring extent of potholing in the Regional Pothole sub-facies (FWP2 potholes)

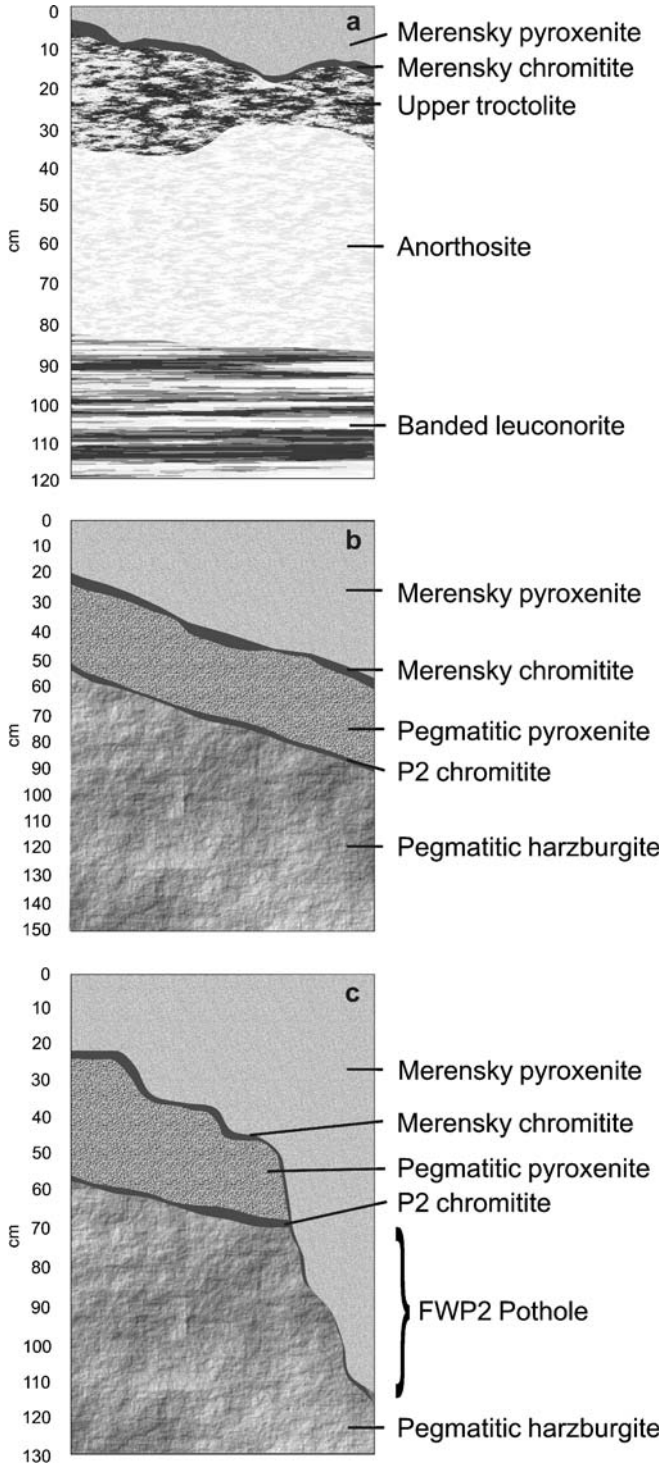

◀ **Fig. 3** Schematic representations of selected reef types in the Regional Pothole sub-facies at Northam Platinum Mine (refer to Fig. 2). **a** NP2 Reef, comprising the base of the Merensky Cyclic Unit (MCU), which consists of a basal chromitite stringer overlain by a medium-grained orthopyroxenite. This is underlain by a variably troctolized, leucocratic footwall, which typically grades downwards, through a laminated leuconorite, into a massive norite. **b** P2 Reef (*slope to the right* represents the regional dip of the reef), consisting of the base of the MCU, as described above, resting on a "reconstituted" or recrystallized pegmatitic pyroxenite, which overlies the Upper Pseudo Reef (P2) stringer chromitite. This is underlain by pegmatitic harzburgite. **c** Margin of a FWP2 pothole/reef type, consisting of the base of the MCU, as described above, which transgresses the lower or P2 chromitite. The margins of FWP2 potholes may be highly irregular, as is the rate of downward transgression of the Merensky Chromitite

Regional Pothole formation. It should be noted that, while such a model may also be applicable to primary and secondary potholing, their elucidation is not the aim of this study.

Statistical analysis

Daily reef mapping and plotting of reef types at a scale of 1:200 has generated an accurate representation of the distribution and form of FWP2 potholes at Northam (Fig. 4). A total of 1,385 FWP2 potholes, with their margins defined as the array of points at which the Merensky Chromitite truncates the Upper Pseudo-Reef chromitite, are quantitatively analyzed in terms of their shape (circularity and dendricity), orientation, and spatial distribution (autocorrelation and Fry analysis). This contributes to a model of FWP2 pothole initiation and growth, which is then compared to existing, largely qualitative models of pothole formation in the "Discussion".

Shape analysis—short vs long axis ratio and long axis orientation

A total of 1,512 FWP2 potholes have been mapped to date. Of these, 1,385 were approximated to simple ellipses and their long and orthogonal short axis dimensions measured, on a 1:1,000 scale map, using a radial scale. The remaining 127 FWP2 potholes were found to be too irregular to approximate to simple ellipses. This section does not take into account the irregularity or dendricity of potholes, which will be treated later using a subset of 638 potholes, which are distributed evenly across the Northam mining lease area. Given that an "infinitesimally small" pothole lies on the zero intercept of a plot of short vs long axis length, the equation of a best fit curve is: x=+ 0.62(y), where 'x' and 'y' are the short and long axis dimensions, respectively, and R^2=0.93 (Fig. 5a). This figure accords well, within 90% confidence, with the arithmetic mean of the short vs long axis ratio (0.63±0.011). It is noted, however, that there is a spread within the data.

To resolve this apparent spread, data were subdivided into several subsets, with divisions at maximum long axis lengths of 10, 15, 20, 30, 35, 40, 45, 50, 60, 70, 80, 90,

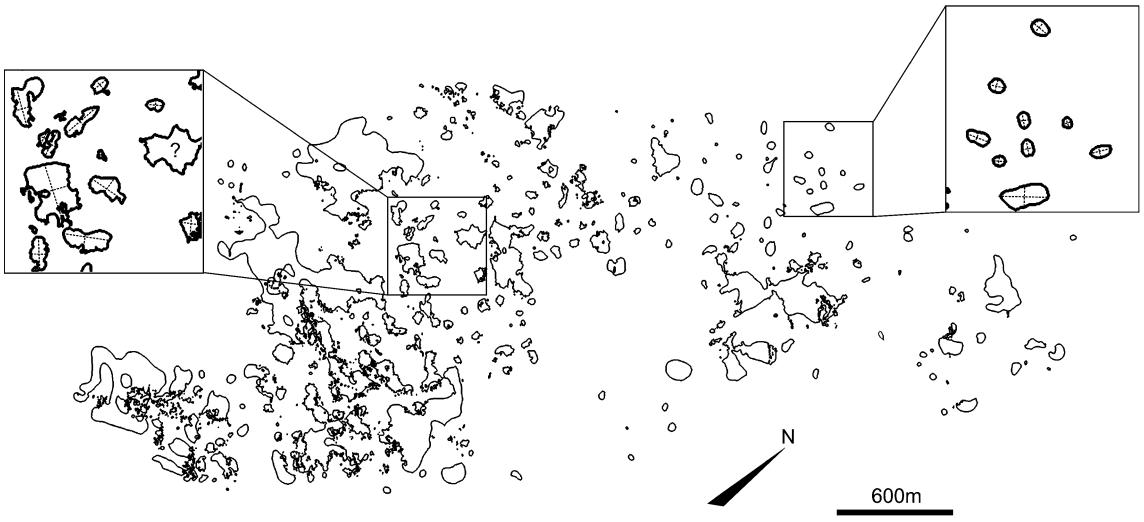

Fig. 4 Plan of the study area showing the larger FWP2 potholes on Northam Platinum Mine (*N*=1,512). The short axis vs long axis ratio for 1,385 of these potholes (see *insets*) was measured on the plane of reef. The proportion of FWP2 potholing increases from NE to SW in mined-out areas. Note the highly irregular (dendritic) shapes of some of the largest potholes, which are not considered for this study due to the difficulty of determining a definite long or short axis

100, 125, 150, 175, 200, and 400 m. The short to long axis ratio was graphically derived for each division, excluding potholes with 1:1 axis ratios and with long axes <6 m (*N*=638 potholes) (Fig. 5b). This ratio increases from 0.48±0.02 to 0.61±0.05 in the long axis range 10 to 60 m, then decreases from 0.61±0.05 to 0.57±0.08 over the long axis range 61 to 100 m, then increases again from 0.57±0.08 to 0.61±0.01 over the long axis range 101 to 400 m. The trend reversals and inflexions on Fig. 5b suggest that the relationship between short vs long axis

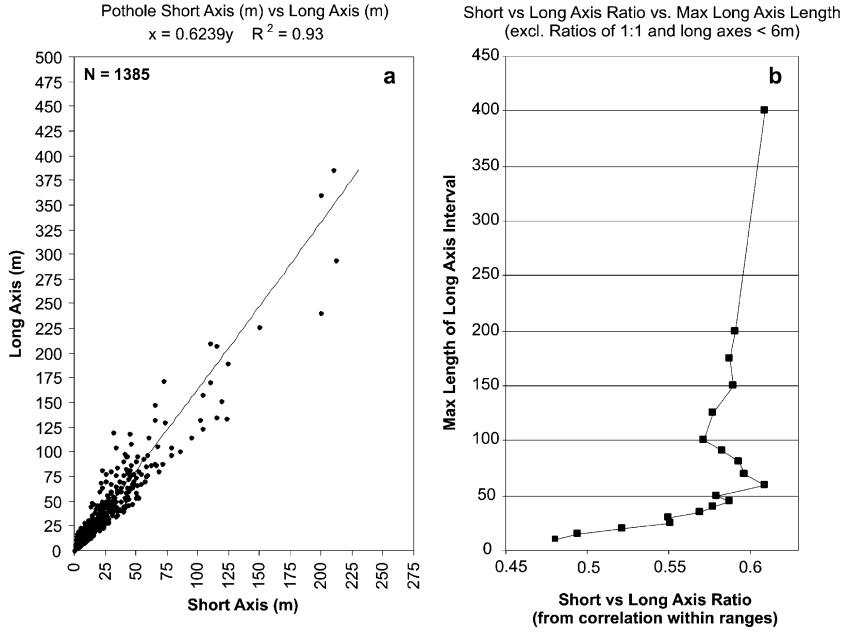

Fig. 5 **a** A plot of the long (*LA*) vs short (*SA*) axes dimensions of FWP2 potholes shows a positive correlation, with SA=0.62×LA (R^2=0.93) for the full data set. Note the data spread with increasing axial length. **b** Division of data into ranges of long axis lengths of 35, 40, 45, 50, 60, 70, 80, 90, 100, 125, 150, 175, 200, and 400 m indicates that there is an irregular but systematic change in the SA to LA ratio with increasing (or maximum) LA length. The SA to LA ratio was graphically derived for each of these divisions. Potholes with 1:1 axis ratios and/or with long axes <6 m are excluded. The ratio increases from approximately 0.52 to 0.61 in the long axis range 10 to 60 m, then decreases from 0.61 to 0.57 over the long axis range 61 to 100 m, then increases again from 0.57 to 0.61 over the long axis range 101 to 400 m. The rates of SA to LA ratio change per absolute change in maximum long axis length are (+) 0.0026, (−) 0.00093, and (+) 0.000124, i.e. systematically decreasing with increasing long axis length

ratio and pothole size is complex. For instance, data suggest that potholes become more circular (i.e., short vs long axis ratio increases) until their long axes reach approximately 60 m. This trend reverses, such that potholes become less circular/more eccentric, until a long axis length of 100 m, after which another trend reversal occurs, although there is little data for potholes with long axes greater than 200 m in length. The rate of change of short vs long axis ratio with respect to long axis length is not constant between the aforementioned inflexion points of Fig. 5b, effectively decreasing with increasing long axis length. The rates of ratio change per absolute change in maximum long axis length are (+) 0.0026, (−) 0.00093, and (+) 0.000124/m. The significance of this is presently unknown.

Shape analysis—pothole shape comparison

Although the majority of potholes may be broadly approximated to ellipses, their margins are nevertheless inherently irregular. Therefore, a method was devised to describe and compare pothole shapes, regardless of their size and potentially irregular margins. Such a method required the derivation of additional shape parameters. A subset of 638 FWP2 potholes, which had short axes longer

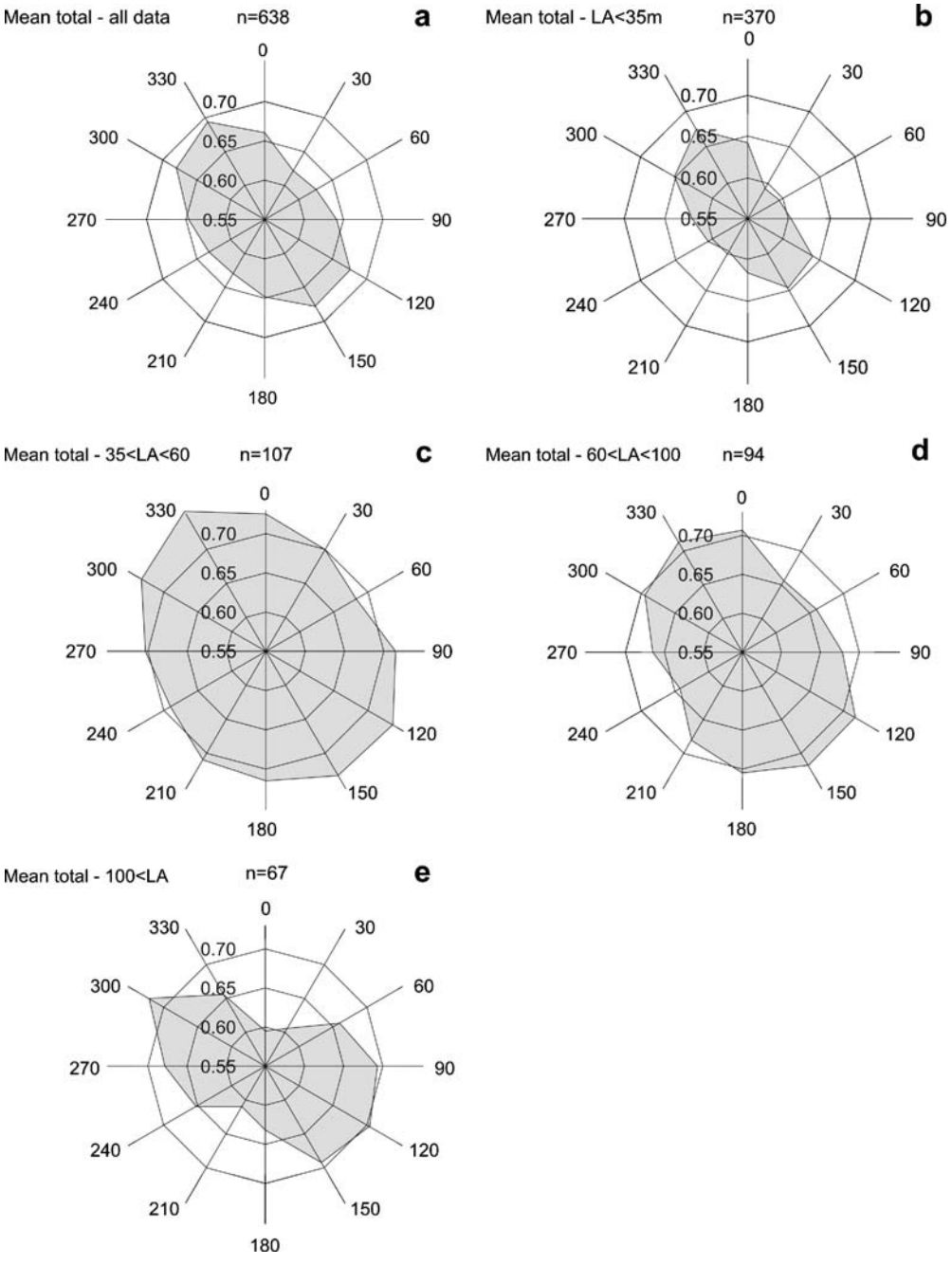

Fig. 6 Pothole shape. **a** "Average normalized" pothole shape for a subset of 638 of the larger potholes (see text for details). SA to LA ratio of 0.917; LA orientation of 120–150°. **b** Average normalized pothole shape for potholes with LA <35 m. SA to LA ratio of 0.906; LA orientation of 120–150°. **c** Average normalized pothole shape for potholes with LA of 35 to 60 m. SA to LA ratio of 0.923; LA orientation of 120–150°. **d** Average normalized pothole shape for potholes with LA of 60 to 100 m. SA to LA ratio of 0.912; LA orientation of 150°. **e** Average normalized pothole shape for potholes with LA >100 m (note bilobate form). SA to LA ratio of 0.854; LA orientation of 120°

than 0.7 m, were selected randomly but equally from every 200×200 m area on the 1:2,000 scale map to provide a representative selection of FWP2 shapes from the entire Northam mining lease area. A radial scale, oriented with 000° to true north, was placed over these potholes and adjusted until its center point was approximately equidistant from opposite pothole edges. The radial distance to the pothole edge was measured at every 30° interval, with the magnitude of the maximum radial length and bearing being noted for each pothole. The value at each 30° interval was then normalized to this maximum radial length. The normalized dimensions for all potholes were collated to generate "average normalized" pothole shapes (Fig. 6). Data for individual potholes were then binned, based on the inflexions in Fig. 5b, into absolute long axis intervals of <35, 35–60, 60–100, and >100 m. Average normalized pothole shapes were generated for long axis intervals (Fig. 6b–d) derived from the inflexion points on short vs long axis plots (i.e., Fig. 5b).

Potholes with long axis lengths of less than 100 m have an average normalized pothole shape of a simple ellipse, elongate on a 120–150° orientation. Potholes with long axis lengths greater than 100 m have an average normalized shape that is bilobate and elongate on a 120° orientation. The average aspect ratio of potholes is highest for potholes with long axis lengths greater than 100 m and lowest for potholes with long axis lengths between 35 and 60 m (Table 1). Long axis orientations were binned into the intervals defined by Fig. 5b (Fig. 7b–e) and were plotted as Rose diagrams (Fig. 7a; Table 2). A composite frequency plot of long axis orientation is shown in Fig. 7f, also binned into the above-mentioned intervals.

The most common long axis orientation for potholes with long axis lengths less than 100 m is 150°, but for potholes with long axis lengths greater than 100 m, this is 120°. The least common long axis orientations are generally 030 and 060°. Potholes with long axis lengths in the range 35 to 60 m have a secondary 030° trend, whilst potholes with long axis lengths of greater than 100 m have a distinct low on the 000° orientation.

Table 1 Summary of normalized pothole shape data for the full subset of 638 potholes (top row) and binned into ranges defined by inflexions in Fig. 5b (subsequent rows)

Interval	Number	LA orientation	Other	SA/LA
All data (subset)	638	120–150		0.917
<35 m	390	120–150		0.906
35–60 m	111	120–150		0.923
60–100 m	81	150		0.912
>100 m	56	120	Low 000–030	0.854

SA Short axis length (m), *LA* long axis length (m)

Table 2 Summary of long axis orientation data for the full subset of 638 potholes (top row) and binned into ranges defined by the inflexions in Fig. 5b (subsequent rows)

Interval	Number	Preferred orientation	Secondary orientation	Frequency of preferred orientation (%)
All data (subset)	638	150		25
<35 m	390	150		26
35–60 m	111	150	030	29
60–100 m	81	120–150		65
>100 m	56	120	Low 000	28

Orientations are in degrees clockwise from true north

Shape analysis—pothole circularity

Circularity or the uniformity/regularity of individual pothole radii was derived from data captured in pothole shape analysis. The circularity test is based on the premise that radial lengths are equal, all normalized radial lengths are equal to 1.0, and the average normalized radial length, $\check{r}$, is also equal to 1.0 for circular potholes. Any deviation from this ideal case denotes a measurable deviation from circularity. The parameters for this are as follows:

– Circular potholes:

$$\breve{r} = \sum \left(r'\right) \Big/ n_r = 1$$

– Non-circular (elliptical) potholes:

$$\breve{r} = \sum \left(r'\right) \Big/ n_r < 1 \textit{and } \breve{r} \rightarrow 2/n_r \textit{with increasing aspect ratio}$$

where $\sum(r')$ is the sum of the normalized radial lengths and n_r is the number of radial measurements. The $\check{r}$ values were binned in 0.1 divisions from $\check{r}$=0.3 to $\check{r}$=1.0 and plotted as a histogram (Fig. 8a). Binned $\check{r}$ data were, in turn, binned for long axis divisions derived from Fig. 5b and for long axis orientations from 000 to 150°, producing composite frequency plots (Fig. 8b,c). Circularity index, $\check{r}$, for the total data set is negatively skewed around a mean of 0.65±0.002 (90% confidence limits). This agrees well with the mean axial ratio and, thus, implies that it is valid to approximate potholes to simple elliptical forms for the purposes of shape analysis. Mean $\check{r}$ is highest for potholes of long axis lengths in the range 35 to 60 m (0.80) and/or with long axis orientations of 150° (0.80).

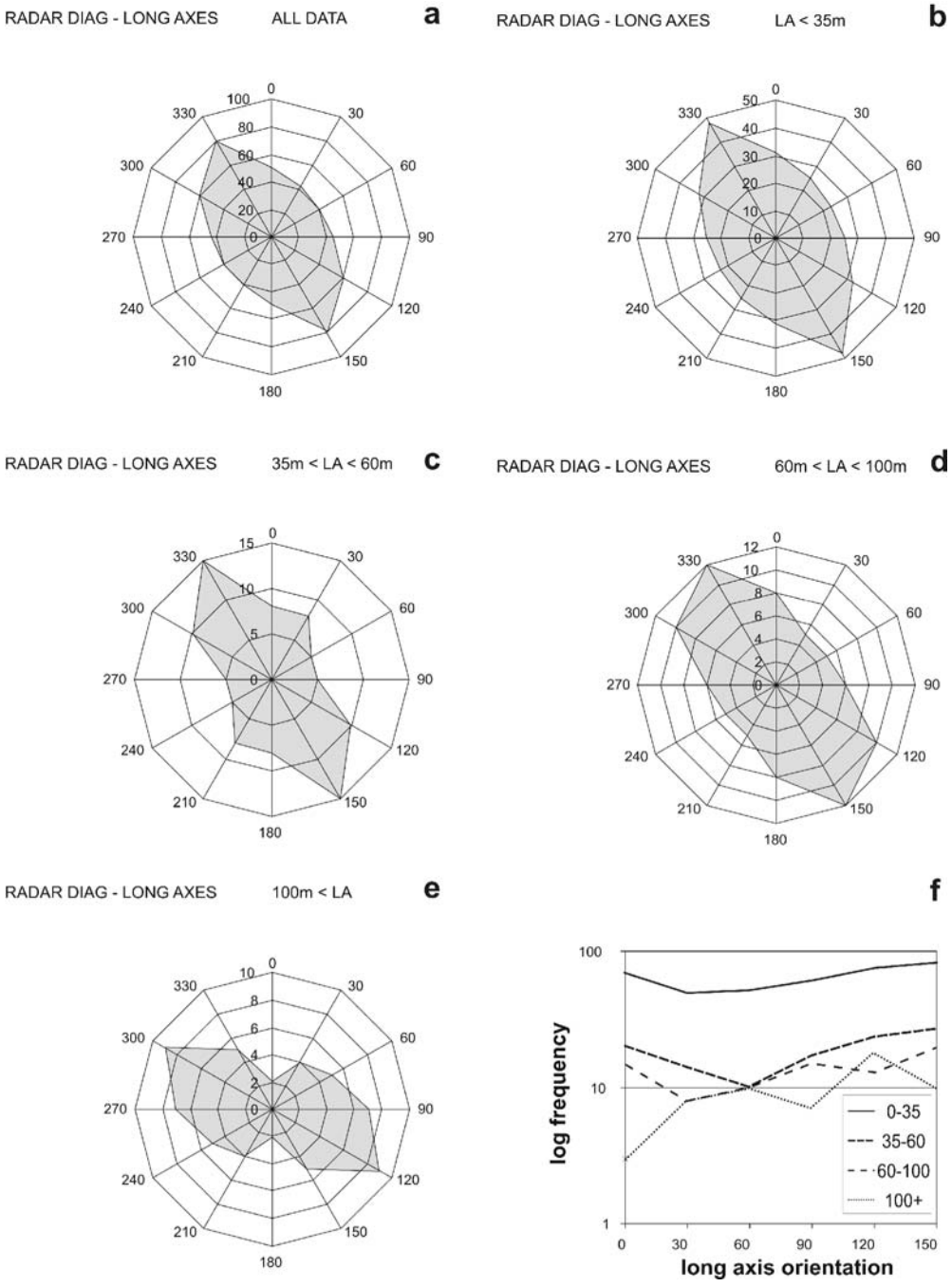

Fig. 7 Long axis orientations. **a** Rose/radar diagram of long axis orientations of a subset of 638 larger potholes (see text for details). The preferred orientation is 150°. **b** Rose/radar diagram of long axis orientations of potholes with LA <35 m. The preferred orientation is 150°. **c** Rose/radar diagram of long axis orientations of potholes with LA of 35 to 60 m. The preferred orientation is 150°. **d** Rose/radar diagram of long axis orientations of potholes with LA of 60 to 100 m. The preferred orientation is 120–150°. **e** Rose/radar diagram of long axis orientations of potholes with LA >100 m. The preferred orientation is 120°. **f** Plot of long axis orientation of potholes, binned into the ranges defined in Fig. 5b, against the log frequency of their occurrence. The preferred orientations are from 120 to 150°

Shape analysis—pothole dendricity

Whether circular or elliptical, a simple pothole form will display bipolar symmetry about its center. The degree to which this symmetry is disrupted is defined as the pothole dendricity, Ď. A test for dendricity, which is independent of long axis orientation, was devised using normalized pothole radial measurements. Within a Cartesian grid, with a *Y* axis running north–south and an *X* axis running east–west, the degree of dendricity is defined as the sum of the absolute radial symmetries about both *Y* and *X* axes. The radial symmetry about an axis is the sum of the absolute variance of opposing radii (Fig. 9). A symmetrical pothole will have Ď=0 but Ď→∞ dendricity/dendricity. Whilst a symmetrical, highly crenulated pothole would have Ď=0, visual inspection of the potholes in the study area revealed no examples of this; indeed, the occurrence of this in nature is deemed to be highly unlikely.

Ď was binned for increments of 0.1 from 0.1 to 2.5 (Fig. 10a). These data were then binned for long axis intervals defined in Fig. 5b, as well as long axis trends from 000 to 150° (Fig. 10b,c). Dendricity index, Ď, is positively skewed about a mean of 0.65. The varying pothole sizes display similar trends; however, small potholes possibly display a bimodal distribution, with a secondary peak at Ď=1.0. There appear to be few potholes with long axis

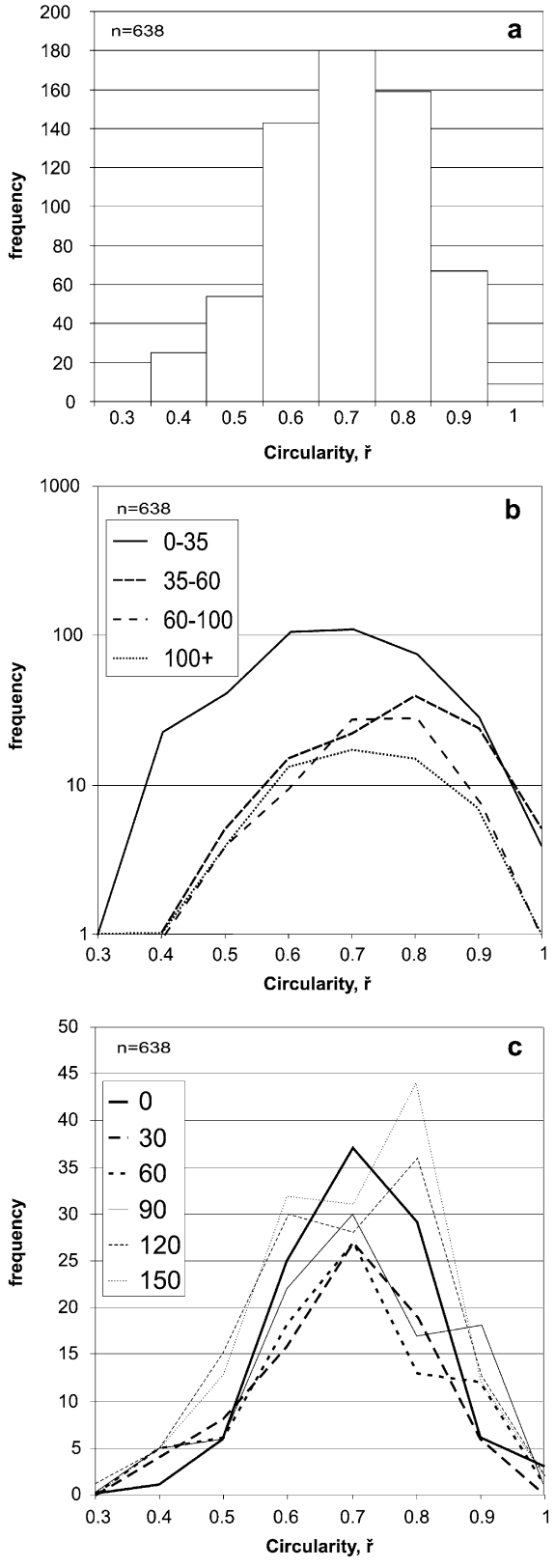

◀ **Fig. 8** Circularity. **a** Frequency plot of circularity, ř (see text for details), showing a negatively skewed distribution and a peak at 0.65. **b** Values of ř binned for long axis intervals defined in Fig. 5b. Mean *ř* is highest for potholes of long axis lengths in the range 35 to 60 m (0.80). **c** Values of *ř* binned for long axis orientations from 000 to 150°; mean *ř* is highest for potholes with preferred long axis orientations of 150° (0.80)

trends of 030° and low values of Ď. Potholes with a long axis trend of 090° display a bimodal Ď distribution.

Distribution analysis–fractal analysis

Fractal analysis (e.g., Turcotte 1991, 1992) and autocorrelation (Fry) analysis (Fry 1979) are two independent statistical approaches to distribution and trend analysis. Each utilizes location or spatial data of point occurrences, in this case in *X*–*Y* space. Fractal geometry is typically applied in several areas of earth sciences and economic geology (e.g., Turcotte 1992; Blenkinsop and Sanderson 1999) to test spatial correlations and distributions over a variety of scales. A point distribution is fractal if it exhibits a geometry that is "self-similar" over a range of different scales (i.e., it is "scale invariant"). To test for spatial invariance and fractal geometry of a point distribution, the box counting method was used, whereby grids with squares of various sizes are superimposed on the point array. For each square size (characterized by the length of one of its sides), the number of squares required to cover all points is calculated. If the distribution pattern of all points is scale invariant, it can be described by a fractal relationship: $N(l)=Cl^{-D}$, where $N(l)$=the number of squares, with side length (l) required to cover all points, C=a constant, and D=fractal dimension (Turcotte 1991). The spatial distribution of the analyzed points is fractal when $N(l)$ plotted against l on a log–log scale results in a straight line with the slope=$-D$. The log–log distribution in Fig. 11a shows a line that is curved at small box sizes due to undersampling of very small potholes and minor reef irregularities. Fractal distributions occur in nature only between certain lower and upper limits and fractal dimensions can only be calculated from the linear portions of the graph. Two fractal dimensions are inferred from Fig. 12; in the l range 168 to 1,935 and 1,935 to 3,869. Corresponding D values are −1.24 and −1.00, respectively. A constant C value, for l in

Table 3 Summary of trends derived from Fry and orientation analysis of pothole center point data

Long axis range	1 (°)	2 (°)	3 (°)	4 (°)	5 (°)	6 (°)	7 (°)	8 (°)	9 (°)
<35 m			045	055	075	107	122	147	
35–60 m		025	040		080	100	123		168
60–100 m	008		030		075			152	
100–400 m			037		072	112			178
Summary trend			038		075	110	122	150	172

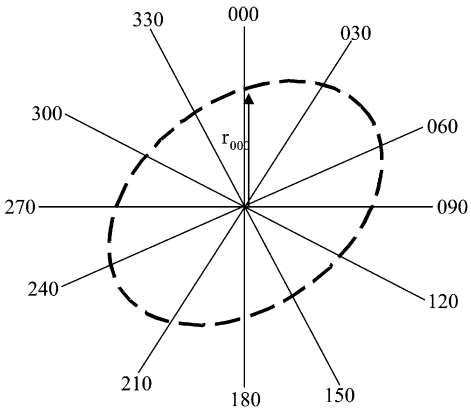

Fig. 9 Dendricity template. Template for the determination of pothole dendricity. Whether circular or elliptical, a simple pothole form will display bipolar symmetry. The degree to which bipolar pothole symmetry (about its approximate center) is disrupted is defined here as the pothole dendricity, Ď. Measured on a Cartesian grid, with the *Y* axis running north–south and the *X* axis running east–west, the degree of dendricity is defined as the sum of the absolute radial symmetries about both *Y* and *X* axes (formulae in *inset*). The radial symmetry about an axis is simply the sum of the absolute variance of opposing radii

the range 168 to 1,935, is 46,995. Lastly, the distribution of the lengths of lines connecting points in the Fry plot is skewed towards larger lengths but shows a peak between 500 and 625 m (Fig. 11b).

Distribution analysis–autocorrelation analysis

Autocorrelation or Fry analysis provides a visual approach to quantifying characteristic spatial trends for a point distribution or groups of point objects. Fry analysis was originally designed to extract strain ellipsoids from groups of deformed objects (e.g., augen or pebbles in deformed sedimentary rocks). However, the technique can also be used to extract linear trends from distributions of point objects. Trends are visually derived from Fry plots. In this study, Fry analysis was applied to the spatial distribution of 1,385 FWP2 pothole centers at Northam Platinum Mine, measured from 1:1,000 scale mine plans.

A Fry plot of the *X*–*Y* coordinates of potholes with long axes <35 m does not give clearly defined trends, partially due to the density of points (Fig. 12a), although dividing the data into long axis length intervals established in Fig. 5b is more instructive (Fig. 12b–d; Table 3). Trends common to all intervals are 038 and 075°, while the trends of 110, 122, 150, and 172° are "intermittent" over the range of data, as are 008, 025, and 055°, which occur once each in the data set. The 008° and 152° trends are observed in the 60–100 m long axis interval. The overall scatter for each Fry plot trends at approximately 040°. Results from all Fry plots were confirmed by orientation diagrams (not shown).

Distribution analysis—chi-squared test

The degree of randomness (lack of fabric or uniformity) or the degree of clustering can be tested with the X^2 (chi-squared) test. This is accomplished by subdividing the area across which the points are distributed into a number of sub-areas of equal size (in this case 100), after which a distribution test is performed for the data. A point distribution is random if the process(es) that control the position of a given point operated independently of the position of all other points. In other words, the process occurred with equal probability in equal subdivisions. A point distribution is uniform if points are distributed with constant density across an area, thereby appearing homogenous. Whereas an extreme form of a uniform distribution is a regular distribution, the introduction of heterogeneities in the distribution pattern results in clustering.

The X^2 test for uniformity yielded an extremely high value of 5,309.602 for the distribution of potholes with long axes of less than 35 m, suggesting that the distribution of smaller potholes is highly non-uniform. This changes when potholes with long axes between 35and 60 m are considered; the X^2 test yields 184.910. Results for the 60 m–100 m and 100 m–400 m ranges are also similarly low (199.677 and 140.286, respectively). This broad, decreasing trend in values derived by the X^2 test suggests that the distribution of potholes becomes progressively less "non-uniform" (i.e., more uniform) with increasing pothole size; however, the distribution never becomes entirely uniform, as would be expected in a natural system.

Discussion—general

Structures such as potholes, slumps, iron-rich ultramafic pegmatites, and "aplites" are generally ascribed to either primary (e.g., Ballhaus 1988) or syn-magmatic processes (e.g., Ferguson and Botha 1963; Carr et al. 1994a) as well as deformation of the Bushveld Complex and the underlying footwall rocks during the latter stages of cooling and crystallization (e.g., Lee 1981).

Proposed controls on sequence disruption include the footwall topography of the cumulate sequence, i.e., the Transvaal Supergroup/Bushveld Complex contact (e.g., Eriksson and Reczko 1995); the variable thickness of major footwall units to the Merensky Reef (Viljoen 1999); the

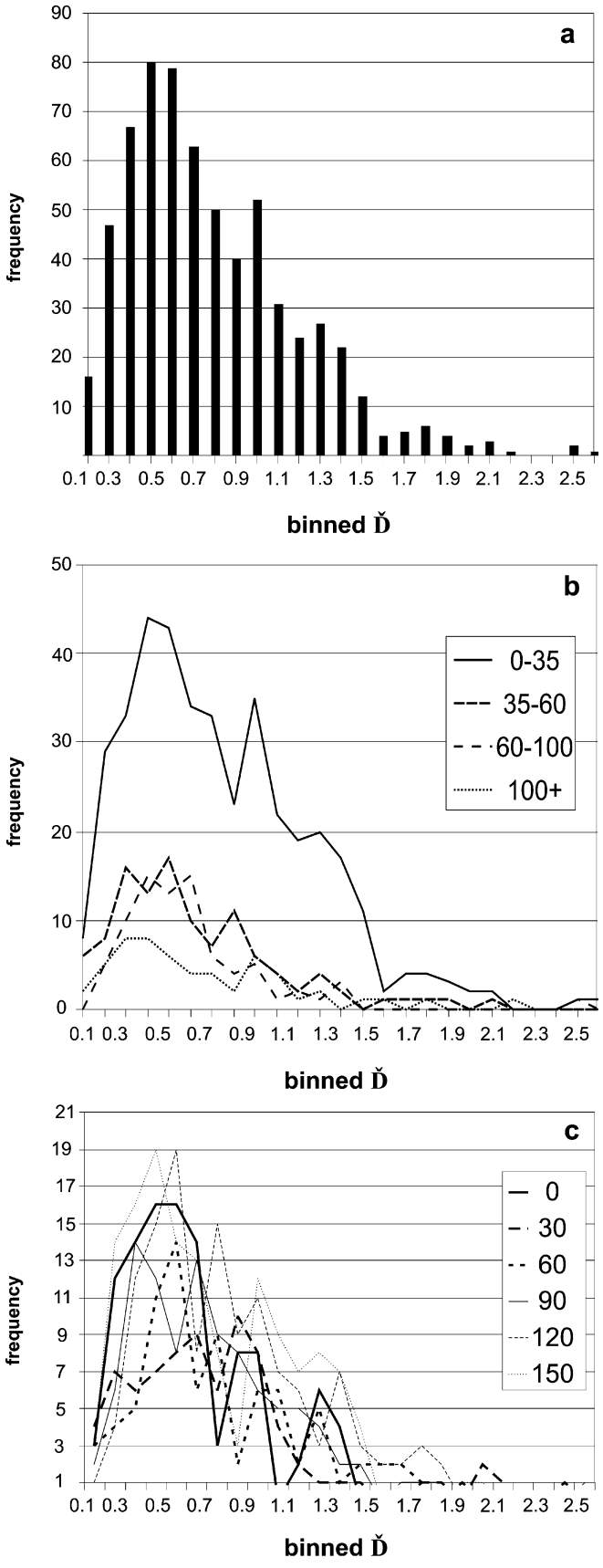

◀ **Fig. 10** Dendricity. **a** Dendricity (Ď) binned for increments of 0.1 from 0.1 to 2.5. Ď is positively skewed about a mean of 0.65. **b** Values of Ď binned for long axis intervals defined in Fig. 5b, showing that smaller potholes (LA <35 m) are more notably skewed towards higher values of Ď. This also implies that larger potholes have higher dendricity. **c** Values of Ď binned according to long axis orientations of their respective potholes (000 to 150°). There appear to be few potholes with long axis trends of 030° and low values of Ď. Potholes with a long axis trend of 090° possibly display a bimodal Ď distribution

proximity of Northam to the Northam "Gap" wherein Upper Zone lithologies are juxtaposed against Main, Critical and Marginal Zone lithologies (Wilson et al. 1994; Viljoen 1999; Reid and Basson 2002); and the effects of local structural features such as pegmatitic, syn- to late-magmatic feldspathic veins and iron-rich ultramafic pegmatites (Lee 1981; Viljoen and Scoon 1985; Scoon and Mitchell 1994; Reid and Basson 2002). The possible effect of syn-magmatic slumping due to steepening of the lateral contacts of the magma chamber, in turn due to syn-magmatic loading, has also been addressed (Carr et al. 1994a,b). Syn-magmatic structures have been attributed to density and viscosity contrasts between the various layers of the cumulate succession, in turn stemming from cumulate mineralogy, fluid content, and interstitial fluid loss due to compaction (Lee 1981). The intricate alternation of lithologies and, therefore, primary density contrasts, together with the presence of primary plagioclase in the Upper Critical Zone, are inferred to be catalysts for syn-magmatic structures (Lee 1981; Ballhaus 1988).

Normal listric faulting, due to stress redistribution in footwall lithologies (mainly the Transvaal Supergroup; Eriksson and Reczko 1995), has been cited as triggering slumping in the cumulate sequence of the Bushveld Complex (Carr et al. 1994a), particularly at higher footwall dips (of up to 45°). Slumping and layer-parallel slip of the partially crystallized cumulate sequence, with down-dip verging folds, has also been proposed for the Western Platinum Mine (Carr et al. 1994a), due to the Bushveld Complex loading the underlying sedimentary host succession. Carr et al. (1994a) suggest that potholes locally form linear trends above the hinge zones of these anticlines/monoclines, which were preferentially melted, thereby supplying linear sources of CO_2-rich fluids and volatiles.

Fluid and volatile escape through the cumulate pile, synchronous with the Merensky Pulse, have been cited as the causes of potholing on the Merensky Reef and "fluid-escape structures" in underlying lithologies (e.g., Campbell et al. 1983; Reid et al. 1993). More reduced mineralization conditions and preferential recrystallization at pothole margins suggest localization of C- and S-rich reducing fluids, symptomatic of "fumeroles", during footwall erosion and MCU deposition (Kinloch 1982; Buntin et al. 1985; Campbell 1986). Ballhaus and Stumpfl (1985) suggested a more widespread, fundamental role for graphite-forming C–O–H–S fluids in the generation of "stratiform" pegmatites, such as those found between chromitite layers in the Merensky Normal Reef. Ballhaus (1988) directly attributed potholes to the large-scale accumulation

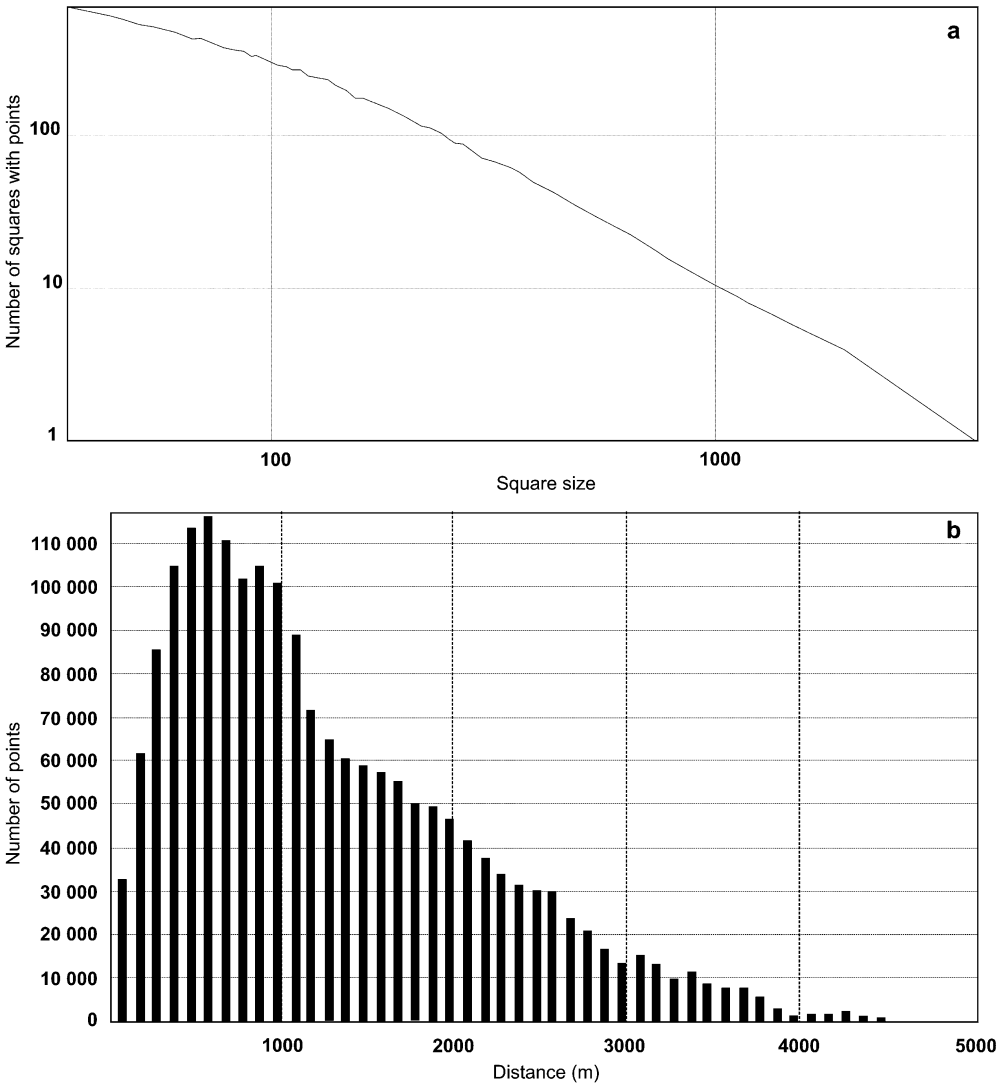

Fig. 11 Fractal analysis. **a** Log–log plot (using pothole center data) of $N(l)$ vs l. This shows a curved distribution at small box sizes, due to the undersampling of very small potholes. The curve does, however, show two linear portions, from which fractal dimensions of 168–1,935 and 1,935–3,869 may be derived (D=−1.24 and −1.00, respectively). The C value for the former range is 46,995. **b** A frequency distribution of the lengths of lines connecting points in the Fry plot for the full data set is skewed towards larger lengths but shows a peak between 500 and 625 m

of dissolved C–H–O–S-rich volatiles and fluids, which locally suppressed the liquidus temperature of plagioclase, resulting in "non-deposition" of anorthositic footwall cumulates. Volatiles and fluids pooled on relatively impermeable footwalls, resulting in locally conformable potholes (Ballhaus 1988), perhaps exemplified by several reef types at Northam Mine (Smith et al. 2004). Potholing is, therefore, a primary feature in the model of Ballhaus (1988). The Merensky Chromitite "drape" and its accompanying cyclic unit, which filled these areas of non-deposition, appear to have been subsequent to or, at best, overlapping with these processes.

The chemical conditions and petrographic nature of the cumulate pile and its interaction with the magma pulse that formed the MCU have been appealed to in the "resorption pit" model (Campbell et al. 1983; Kruger and Marsh 1982; Campbell 1986). Resorption is due to the entry of the "Merensky magma pulse" into the magma chamber. The plagioclase-undersaturated Merensky pulse may have locally resorbed and removed pre-existing cumulates. Anorthosites and leuconorites were apparently more vulnerable to resorption, while their ductile nature (Viljoen 1999) might also have made them prone to preferential magma current erosion (Schmidt 1952; Ferguson and Botha 1963).

Iron-rich ultramafic pegmatites (IRUPs) in the form of veins, pipes, and subconcordant sheets disrupt the cumulate sequence of the Upper Critical Zone (Scoon and Mitchell 1994; Viljoen and Scoon 1985; Reid and Basson 2002). IRUPs preferentially replace plagioclase-rich cumulates beneath the Merensky Chromitite (the base of the MCU) but spread laterally and pond against relatively impermeable chromitite layers. IRUPs are spatially associated with potholes and are notably more abundant towards the Northam Gap (D. Smith, personnal observation).

Models for potholing of the Merensky Reef must take into account a variety of factors, including the syn-magmatic composition of the cumulate pile; the energy and composition of the Merensky magma pulse; deformation, compaction, and devolatilization of the underlying cumulate sequence; and the dip and topography of footwall rocks to the Bushveld Complex. As most of the immediate footwall cumulates have been removed and/or recrystal-

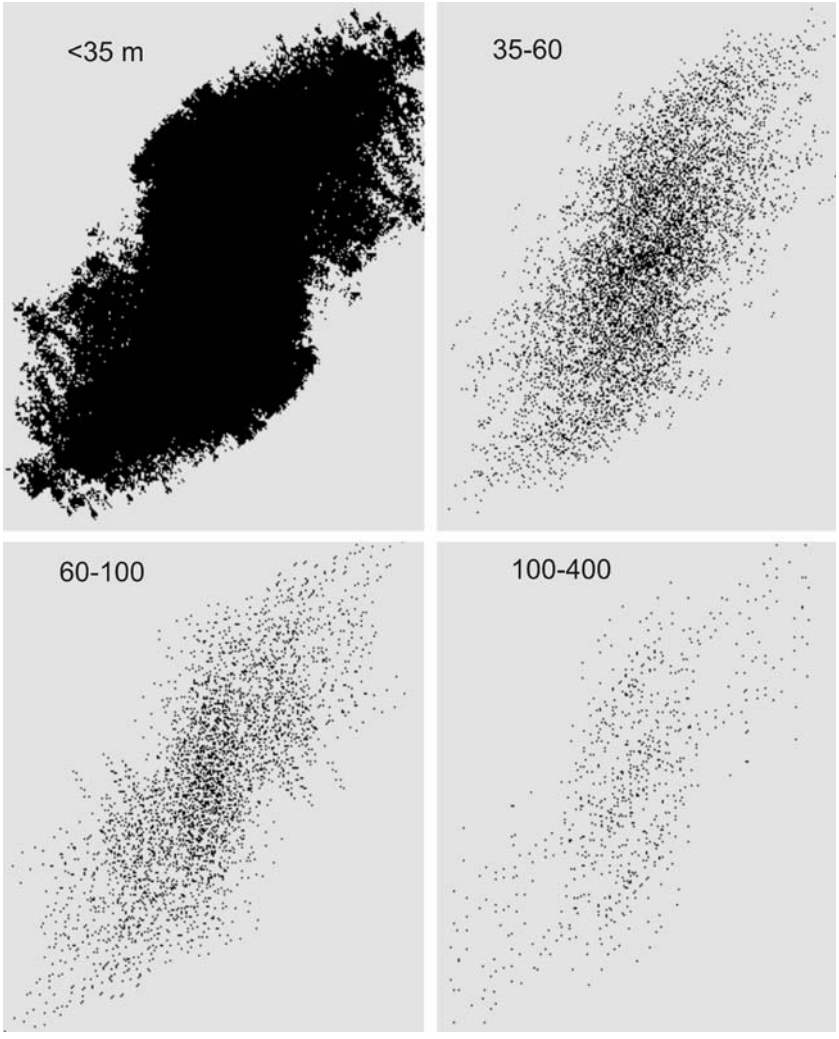

Fig. 12 Fry plots (translation diagrams). **a**–**d** Fry plots generated from pothole center positions, for long axis length intervals of <35, 35–60, 60–100, and >100 m (using software of Kuskov et al. 2001). The trends derived from the Fry plots are supported by orientation diagrams. The principal trends/orientations derived from these are detailed in Table 3

lized due to potholing and the imposition of an apparently high-temperature "Merensky magma pulse", linked or potentially causative, underlying features may have been destroyed or modified beyond recognition (Smith et al. 2004). There is certainly little direct evidence, in rocks exposed by development mining before reef extraction, for underlying or preemptive structures related to Merensky Reef potholes. Alternatively stated, larger-scale, more fundamental controls may have been operative. "Potholes" (sensu lato) and related features may take a variety of forms across the Bushveld Complex and, consequently, their catalysts may have been highly variable in nature and operative over a great variety of scales and time intervals. It is pertinent that none of the abovementioned studies adopt a rigorous quantitative analysis of the inter-relationships between pothole distribution and shape.

Discussion—model

The model which best fits the observed shape and distribution of FWP2 potholes is a combination of independent growth and "nearest neighbor" merging along specific orientations, coincident with regional structural trends (Fig. 13). Three prevalent structural trends are present: Pilanesberg (150°), Great Dyke (020°), and Murchison (080–110°). Smaller FWP2 potholes (long axis lengths <35 m) display highly variable long axis orientations, have centers aligned along multiple trends, and show a relatively low short vs long axis ratio (0.48±0.02). Primary independent growth caused merging of "nearest neighbor" FWP2 potholes, along a variety of trends. The apparently clustered distribution of original pothole centers allowed for merged potholes with long axis lengths of up to 60 m, exhibiting short vs long axes ratios of 0.61±0.05, preferred orientations of 150° (Pilanesberg), and alignment along 010° (Great Dyke) and 150° (Pilanesberg) trends. Further independent growth of FWP2 potholes allowed for preferential merging of neighboring potholes along new trends, generating potholes with long axes of up to 100 m in length and exhibiting short vs long axes ratios of 0.57±0.08, a preferred long axis orientation of 150° (Pilanesberg) and alignment along trends of 010° (Great Dyke), 040° (local trend), 075° (Murchison), and 150° (Pilanesberg). In turn, preferential merging of these FWP2 potholes, generating potholes with long axes greater than 100 m in length,

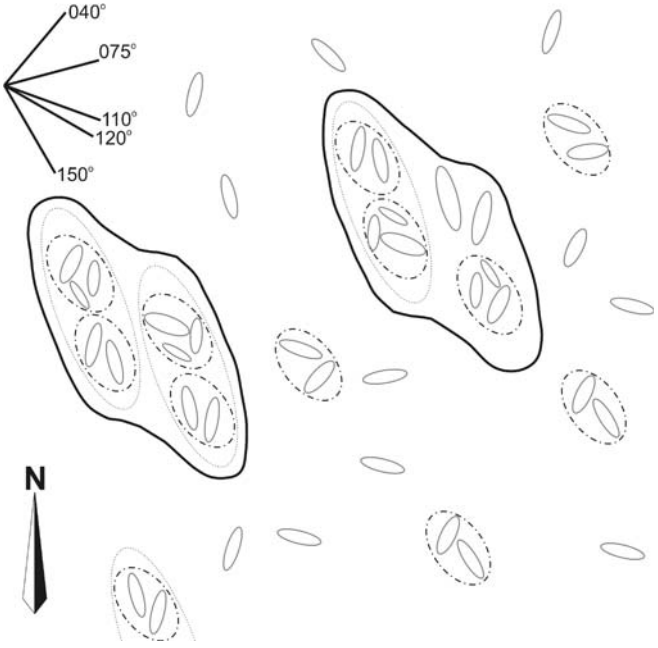

Fig. 13 Model. The growth of potholes is proposed to be a consequence of primary, independent growth and merging of "nearest neighbor" potholes along a variety of trends. The clustered distribution of the original pothole centers provided for merged potholes with long axes lengths of up to 60 m, which exhibited short vs long axes ratios of 0.61, preferred orientations of 150°, and alignment along 010 and 150° trends. Further independent growth caused merging of similar-sized (and smaller) neighboring potholes along the given trends, generating potholes with long axes of up to 100 m in length, preferred long axis orientations of 150°, and alignment along trends of 010, 040, 075, and 150°. In turn, preferential merging of potholes, with long axes greater than 100 m in length, occurred along an orientation of 120°

occurred along a 120° (Murchison) trend. Such potholes exhibit short vs long axes ratios of 0.61±0.01 and preserve a bilobate form. The end of this growth stage is considered to be the termination of FWP2 pothole formation. As an aside, the total volume of the cumulate pile redistributed through the process of regional potholing within the Northam Platinum mine lease area is in the order of 0.536 km^3, which represents a mass of 1,607 Mt, using average densities. Of this volume, only 0.011 km^3 or 2% was the result of FWP2 potholing.

The model presented above implies that underlying linear or structural catalysts/controls govern the means whereby FWP2 potholes form and grow, predominantly by merging with other potholes. There are consequently two different yet related variations to the model presented above. Firstly, persistent or reactivated linear controls along the orientations of 040° (local trend) and 075° and 110° (Murchison) influence the shape, orientation, and distribution of FWP2 potholes, while intermittent linear controls with orientations of 010° (Great Dyke) and 150° (Pilanesberg) only become effective at certain FWP2 pothole sizes. This implies that the influence of a linear control with a specific orientation is dependent upon the aerial extent of a given FWP2 pothole and, in turn, its state of growth at the time. Secondly, underlying linear controls impact on FWP2 pothole nucleation. Early FWP2 pothole shape and distribution may have modified magma flow characteristics at the magma–cumulate interface. Turbulent flow over irregularities may have, in turn, enhanced specific pothole orientations in a feedback mechanism. Both variations, as described above, imply that pothole growth is a protracted event or a protracted series of events.

Acknowledgements The authors acknowledge the assistance of Julius Maseko, Francis Motlalentoa, and Armando Langa in gathering data for pothole shape analysis. Debbie Oberholzer provided invaluable assistance in generating pothole plans. Northam Platinum Limited is thanked for their permission to publish this work. Grant Cawthorn, Bernd Lehmann, and an anonymous reviewer are thanked for insightful comments on an earlier draft of this paper.

References

Ballhaus CG (1988) Potholes of the Merensky Reef at Brakspruit Shaft, Rustenburg Platinum Mines: primary disturbances in the magmatic stratigraphy. Econ Geol 83:1140–1158

Ballhaus CG, Stumpfl EF (1985) Occurrence and petrological significance of graphite in the Upper Critical Zone, Western Bushveld Complex, South Africa. Earth Planet Sci Lett 74:58–68

Blenkinsop TG, Sanderson DJ (1999) Are gold deposits in the crust fractals? A study of gold mines in the Zimbabwe Craton. In: McCaffrey KJW, Lonergan L, Wilkinson JJ (eds) Fractures, fluid flow and mineralization. Geological Society Special Publications 155, pp 141–151

Buntin TJ, Granddstaff DE, Ulmer CG, Gold DP (1985) A pilot study of geochemical and redox relationships between potholes and adjacent Merensky Normal Reef of the Bushveld Complex. Econ Geol 71:1299–1307

Campbell IH (1986) A fluid dynamic model for the potholes of the Merensky Reef. Econ Geol 81:1118–1125

Campbell IH, Naldrett AJ, Barnes SJ (1983) A model for the origin of the platinum-rich horizons in the Bushveld and Stillwater complexes. J Petrol 24:133–165

Carr HW, Groves DI, Cawthorn RG (1994a) The importance of synmagmatic deformation in the formation of Merensky Reef potholes in the Bushveld Complex. Econ Geol 89:1398–1410

Carr HW, Groves DI, Cawthorn RG (1994b) Controls on the distribution of Merensky Reef potholes at the Western Platinum Mine, Bushveld Complex, South Africa: implications for distributions of the layering and pothole formation in the complex. S Afr J Geol 97:431–441

Cawthorn RG, Boerst KD (2002) Origin of the Merensky pegmatitic pyroxenite, Bushveld Complex. Extended Abstracts, 9th International Platinum Symposium, Billings, Montana

De Bruin JD (2002) Pothole structures within the Bushveld Complex on Impala Platinum Mine. Extended Abstracts, IAGOD 11, Windhoek, Namibia

Eales HV, Cawthorn RG (1996) The Bushveld Complex. In: Cawthorn RG (ed) Layered intrusions. Elsevier, Amsterdam, pp 181–230

Eales HV, Reynolds IM (1986) Cryptic variations within chromitites of the Upper Critical Zone, Northwestern Bushveld Complex. Econ Geol 81:1056–1066

Eales HV, Botha WJ, Hattingh PJ, de Klerk WJ, Maier WD, Odgers ATR (1993) The mafic rocks of the Bushveld Complex, a review of emplacement and crystallization history, and mineralization, in the light of recent data. J Afr Earth Sci 16:121–142

Eriksson PG, Reczko BFF (1995) The sedimentary and tectonic setting of the Transvaal Supergroup floor rocks to the Bushveld Complex. J Afr Earth Sci 21(4):487–504

Farquhar J (1986) The Western Platinum Mine. In: Anhaeusser CR, Maske S (eds) Mineral deposits of Southern Africa, V. II, Geological Society of South Africa, pp 1135–1142

Ferguson J, Botha E (1963) Some aspects of igneous layering in the basic zones of the Bushveld Complex. Verh Geol Ver S-Afr 64:259–282

Fry N (1979) Random point distributions and strain measurement in rocks. Tectonophysics 60:89–105

Kinloch ED (1982) The regional trends in platinum-group mineralogy of the Critical Zone of the Bushveld Complex, South Africa. Economic Geology 77:1328–1347

Kruger FJ (1990) The stratigraphy of the Bushveld Complex: a re-appraisal and relocation of the Main Zone boundaries. S Afr J Geol 94:376–381

Kruger FJ (1994) The Sr-isotopic stratigraphy of the western Bushveld Complex. S Afr J Geol 97:393–398

Kruger FJ, Marsh JS (1982) Significance of the $^{87}Sr/^{86}Sr$ ratios in the Merensky cyclic unit of the Bushveld Complex. Nature 289:53–55

Kuskov A, Mikhailov A, Dirks P (2001) DotProc v. 1.3. The analysis of 2-dimensional data sets. Computer shareware (http://dotproc.fromru.com)

Lee CA (1981) Post-deposition structures in the Bushveld Complex mafic sequence. J Geol Soc (Lond) 138:327–341

Lee C (1996) A review of mineralization in the Bushveld Complex and some other layered intrusions. In: Cawthorn, R.G. (ed.) Layered Intrusions, Elsevier, Amsterdam, 103–145

Leeb-Du Toit A (1986) The Impala Platinum Mines. In: Anhaeusser CR, Maske S (eds) Mineral deposits of Southern Africa, V. II, Geological Society of South Africa, pp 1091–1106

Maier WD, Eales HV (1997) Correlation within the UG2–Merensky Reef interval of the western Bushveld Complex, based on geochemical, mineralogical and petrological data. Bulletin of the Geological Survey of South Africa 120, 56 pp

Mossom RJ (1986) The Atok Platinum Mine. Anhaeusser CR, Maske S (eds) Mineral deposits of Southern Africa, V. II, Geological Society of South Africa, pp 1143–1154

Reid DL, Basson IJ (2002) Iron-rich ultramafic pegmatite replacement bodies within the Upper Critical Zone, Rustenburg Layered Suite, Northam Platinum Mine, South Africa. Mineral Mag 66(6):895–914

Reid DL, Cawthorn RG, Kruger FJ, Tredoux M (1993) Isotope and trace-element patterns below the Merensky Reef, Bushveld Complex, South Africa: evidence for fluids? Chem Geol 106:171–186

Schmidt ER (1952) The structure and composition of the Merensky Reef and associated rocks in the Rustenburg platinum mine. Verh Geol Ver S-Afr 55:234–279

Scoon R, Mitchell A (1994) Discordant iron-rich ultramafic pegmatites in the Bushveld Complex and their relationship to iron-rich intercumulus and residual liquids. J Petrol 35:881–917

Smith DS, Basson IJ, Reid DL (2004) The Normal Reef sub-facies of the Merensky Reef at Northam Platinum Mine, Zwartklip Facies, Western Bushveld Complex. Can Mineral 42:243–260

Turcotte DL (1991) Fractals in geology: what are they and what are they good for? GSA Today 1:1–4

Turcotte DL (1992) Fractals and chaos in geology and geophysics. Cambridge University Press, 196 pp

Viljoen MJ (1994) A review of regional variations in facies and grade distribution of the Merensky Reef, western Bushveld Complex, with some mining implications. Proceedings of the 15th CMMI Congress, South African Institute of Mining and Metallurgy, pp 183–194

Viljoen MJ (1999) The nature and origin of the Merensky Reef of the western Bushveld Complex based on geological facies and geophysical data. S Afr J Geol 102(3):221–239

Viljoen MJ, Scoon N (1985) The distribution and main geologic features of discordant bodies of iron-rich ultramafic pegmatite in the Bushveld Complex. Econ Geol 80:1109–1128

Viljoen MJ, Hieber R (1986) The Rustenburg Section of Rustenburg Platinum Mines Limited, with reference to the Merensky Reef. In: Anhaeusser CR, Maske S (eds) Mineral deposits of Southern Africa, V. II, Geological Society of South Africa, pp 1107–1134

Viljoen MJ, Theron J, Underwood B, Walters BM, Weaver J, Peyerl W (1986a) The Amandelbult Section of Rustenburg Platinum Mines Ltd, with reference to the Merensky Reef. In: Anhaeusser CR, Maske S (eds) Mineral deposits of Southern Africa, V. II, Geological Society of South Africa, pp 1041–1060

Viljoen MJ, De Klerk WJ, Coetzer PM, Hatch NP, Kinloch P, Peyerl W (1986b) The Union Section of Rustenburg Platinum Mines Ltd, with reference to the Merensky Reef. In: Anhaeusser CR, Maske S (eds) Mineral deposits of Southern Africa, V. II, Geological Society of South Africa, pp 1061–1090

Viring RG, Cowell MW (1999) The Merensky Reef on Northam Platinum Limited. S Afr J Geol 102(3):192–208

Von Gruenewaldt G (1977) The mineral resources of the Bushveld Complex. Miner Sci Eng 9:83–95

Wagner PA (1929) Platinum deposits and mines of South Africa. Struik, Cape Town, South Africa, 383 pp

Wilson AH, Chunnett GK (2002) Type variations in the Merensky Reef in the western Bushveld Complex: critical comparisons of the geochemistry, textures and metal distributions. Extended abstracts, 9th international platinum symposium, Billings, Montana

Wilson JR, Cawthorn RG, Kruger FJ, Grundvig S (1994) A major unconformity in the western Bushveld Complex: the northern "gap". S Afr J Geol 97:462–472